

## Improvement of Thermal Stability and Electrical Properties of Polyaniline through Hybrid Nanocomposites PANi/PVA/CaO

Osama Saber, Sobhy S. Ibrahim, Mohamed Abu-Abdeen, Adil Alshoaibi,  
and Abdullah El-Naeim

Physics Department, Faculty of Science, King Faisal University, Al-Hassa 31982,

Received 9 May 2018 - Accepted 2 January 2019

### ABSTRACT

Single polymer cannot achieve all demands to advance new technologies. Therefore, the combination of two or more polymers or metal oxides leads to a polymer with superior properties compared to that of the discrete components. Hence, the present study aims to improve both the electrical properties and the thermal stability of polyaniline through three nanocomposites based on organic-inorganic nanohybrids. Three nanocomposites were prepared with different weight ratios of polyaniline to polyvinyl alcohol and fixed weight ratio of calcium oxide nanoparticles. The thermal analyses showed higher thermal stability of the three phase nanocomposites compared to the protonated polyaniline. Both DC and AC electrical characterizations showed that the highest concentration of polyaniline gave a semi-metallic behavior for polyvinyl alcohol at low voltages. Also, the AC parameters ( $Z'$ ,  $Z''$ ) showed varying behaviors for all the prepared nanocomposites at different temperatures. Where, the impedance of the nanocomposite increased in the temperature range from 30 °C to 80 °C and then decreased monotonically from 90 °C to 140 °C. This electrical behavior showed very interesting outcomes, which opens up new horizons for many applications for such three phase composites, especially in the field of electronics and sensors.

**Key Words:** Electrical properties, Nanocomposites, PANi/PVA/CaO, Thermal stability.

### INTRODUCTION

Polyaniline (PANi) is one of the most promising conducting polymers. This is due to its low cost, good electrical properties, and environmental stability. Various industrial applications depend on this polymer, such as actuators (Hien *et al.*, 2017, Graboski *et al.*, 2018), sensors (Guo *et al.*, 2018), supercapacitors (Tavares *et al.*, 2018), and transistor beside its capability to absorb electromagnetic waves which make it a candidate for electromagnetic shielding applications (Hoghoghifard *et al.*, 2018; Sun *et al.*, 2018). However, the uses of unsubstituted PANi are limited because of its infusibility and insolubility (Hatamzadeh *et al.*, 2012). It is known that PANi in emeraldine salts is insoluble but conductive while its emeraldine base form is an insulator and it can dissolve in some polar organic solvents, such as N-methylpyrrolidone and dimethylsulfoxide. The rigidity of the main chain of PANi leads to lack of its solubility. In addition, the existence of conjugated electronic structure in the main structure of PANi causes resistance to the solubility

process. Consequently, in order to increase the solubility of PANi, a versatile and easy technique depending on intercalation of sulfonic groups on PANi chain was effective toward soluble conductive PANi.

The emeraldine base form of PANi was treated by fuming sulfuric acid to produce soluble sulfonated or protonated PANi. However, the electrical conductivity of the resultant PANi was reduced after sulfonation (Jaymand 2013). This reduction of conductivity was due to reduction of the electrons density at the PANi backbone because of electrons withdrawing effect of the sulfonic groups (negative resonance effect).

To avoid this main drawback, many researchers (Bhadra *et al.*, 2017) investigated the effect of blending PANi with other insulating polymers on the mechanical, rheological, and thermal properties of PANi. The protonated PANi blend in different insulating polymers such as polymethyl methacrylate (Gao *et al.*, 2017), polyvinyl chloride and polyvinyl alcohol (PVA) (Afify *et al.*, 2018) have been investigated during the last few years. The DC & AC

conductivity and dielectric relaxation of PANi/PVA blends were reported by different researchers (Shahin *et al.*, 2017). Other researchers illustrated the effect of adding a third element to form three-phase polymer blend composite for more modification and applications (Singh *et al.*, 2016).

Three phase PANi/PVA nano-composites based on graphene oxide were prepared by electrospinning method to enhance their antibacterial properties (Ghobadi *et al.*, 2016). PANi/PVA electrodes containing active carbon were used for supercapacitor applications (Olad and Gharekhani 2016). The sensing properties of MnO<sub>2</sub>-PANi/PVA thin films for ammonia were investigated by Dupare *et al.* (2013). Hybrid composite of PANi/PVA/TiO<sub>2</sub> as a chemical sensor was studied toward methanol by Subramanian *et al.* (2012).

Although many researchers have developed PANi through three phase nanocomposites, no one studied the effect of the presence of calcium oxide in PANi and their blends. In addition, calcium oxide is known as an inexpensive solid source of protons (Mat and Liong 2009) and is suitable for PANi to facilitate the process of protonation. Calcium oxide (CaO) is a hygroscopic oxide and one of the proton conducting material that has been used in fuel cells as a solid source of protons (Breeze *et al.*, 1998; Daiko *et al.*, 2006).

Thus, this study has converted the PANi after sulfonation into three phase nanocomposites based on PVA and calcium oxides nanoparticles. PVA has polar function groups that facilitate the solubility process in water and the charge transfer. In addition, calcium oxides nanoparticles are used as a filler to improve the thermal stability and the electrical properties of PANi.

In the present article, neutral phase PANi (emeraldine) is doped with sulfonic groups and converted into three phase nanocomposite. Calcium oxide nanoparticles are used as a filler with different percentages of PANi-PVA blend to form three hybrid

nanocomposites. The thermal stability and decomposition of the hybrid nanocomposites are investigated. In addition, the DC and AC electrical properties are studied at different temperatures.

## MATERIALS AND METHODS

PANi, emeraldine base (average molecular weight 100000) and PVA (fully hydrolyzed; molecular weight approximately 30000) were used as starting materials to form polymer blend. Calcium oxide nanopowder ( $\leq 160$  nm) was used as filler for the polymer blend to synthesize three hybrid nanocomposites. Sulphuric acid (99.9%) was used for protonation of the emeraldine base of PANi. These materials were supplied by Sigma–Aldrich, Germany.

0.125, 0.25 and 0.5 g of neutral phase PANi (emeraldine) were used as starting material for preparing three hybrid nanocomposites S1, S2 and S3 with different weighed ratios of poly vinyl alcohol and calcium oxide nanoparticles 2.0:1.0:0.4, 1.0:1.0:0.4, and 0.5:1.0:0.4; respectively. A specific volume (0.3 ml) of sulphuric acid was added to each of the previous weighed samples with stirring using a glass rod to get a homogenous paste of the mixture. Each sample was diluted with 0.6 ml of distilled water with continuous stirring to get a homogenous mixture. A fixed weight (100 mg) of calcium oxide nanoparticles was added to each sample in ultrasonic bath for 30 min. By vigorous stirring, homogeneous solution was attained after 24 h. 0.25 g of PVA was dissolved in water and added to the previous mixture. The mixtures were poured in dishes and dried at room temperature.

## RESULTS AND DISCUSSION

### Thermal Analyses

Thermal gravimetric analysis (TGA) is one of the thermal analyses, which describes the effect of temperature on the rate weight loss of materials. The thermal stability of the prepared materials was characterized by TGA. It was carried out in TA

thermogravimetric analyzer (series Q500) under  $N_2$  atmosphere.

Figure (1) showed that the behavior of the PANi neutral phase (emeraldine) significantly differs from the PANi after protonation with acid. It indicated high thermal stability for PANi insulating phase (emeraldine) and low thermal stability for the protonated conducting PANi agreeing with the results of several reports (Lesueur *et al.*, 1997; Albu *et al.*, 2016). Where, PANi insulating phase (emeraldine) has two thermal decomposition stages while three decomposition steps were observed for the protonated conducting PANi. The first step is due to vaporization of

water molecules. The decomposition of the protonated component of the polymer has occurred through the second step. Finally, the decomposition of polymer backbone chains has happened at higher temperature. Compared with the protonated conducting PANi, the TG curve of the hybrid nanocomposites (PANI/PVA/CaO) showed high thermal stability as shown in Figure (1). The thermal decomposition curve of the nanocomposite was composed of three distinct regions. The weight loss in the first region of the nanocomposite (15%) was less than that of the protonated PANi (35%).

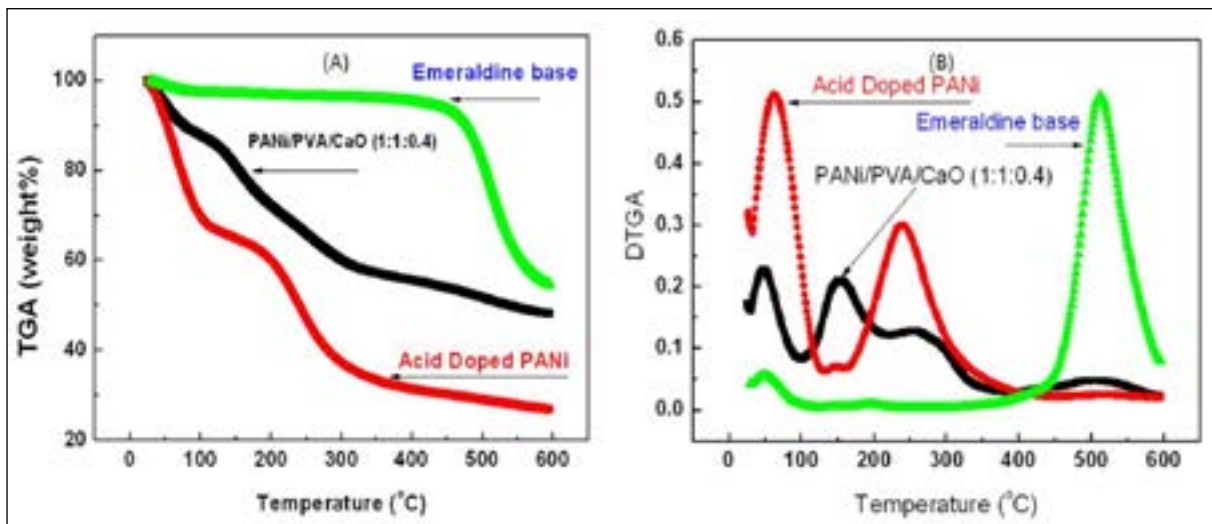


Fig. 1. (A) TGA and (B) DTGA analyses for the emeraldine base, the acid doped PANi and the PANi/PVA/CaO nanocomposite.

This difference could be attributed to existence of inorganic species inside the structure of nanocomposite (Sultana *et al.*, 2013). Where, calcium oxide nanoparticles have high thermal stability. Also, they reduced the amount of the remainder acid which produced acceleration of polymer chain cession. By further heating at 300 °C, the second weight loss of the nanocomposite was 46% while a weight loss 63% was observed for the protonated PANi. With continuing heating to the higher temperature of 500 °C, the protonated PANi lost 70% of its weight and only 51% of the nanocomposite was observed. It indicated that the residual of the protonated PANi was about 24%

while for the nanocomposite was about 49%. The high residual of the nanocomposite confirmed that the high thermal stability of the nanocomposite was attributed to the presence of CaO nanoparticles.

The high thermal stability of the PANi/PVA/CaO nanocomposite was attributed to the interaction between the filler (CaO) and the polymer matrix agreeing with the previous reports of PANi/montmorillonite nanoparticles (Gök *et al.*, 2007), PANi/Ag nanoparticles (Salem *et al.*, 2016), PANi/ZnO (Layeghi *et al.*, 2016) and PANi/CNTs (Saadattalab *et al.*, 2016). It concluded that the addition of CaO nanoparticles plays the main factor for increasing the thermal

stability of the protonated PANi.

From the first derivative of TGA curves (see Figure (1B)), the decomposition processes could be easily monitored through the peak of maximum decomposition rates. For emeraldine, it is clear that two processes have occurred, one is at  $T < 100$  °C, which represented the moisture evaporation (unbounded water) and the other is the main decomposition of the backbone chains of PANi at 520 °C. For the protonated PANi, three peaks were observed at lower temperatures. These peaks represented vaporization of water and decomposition of the protonated PANi chains through two steps; respectively.

The DTGA curve for the nanocomposite (PANi/PVA/CaO) showed a more complicated behavior than the other two samples. Where, two overlapped processes were observed at 154 °C and 253 °C for the main decomposition process. This main decomposition region could be analyzed using peak separation as shown in Figure (2). The first and fourth peaks were due to water evaporation and the decomposition of emeraldine remainder. The second and third peaks were attributed to the decomposition of both PANi (de-doping) () and PVA; respectively (Avlyanov 1999, Pingan *et al.*, 2017).

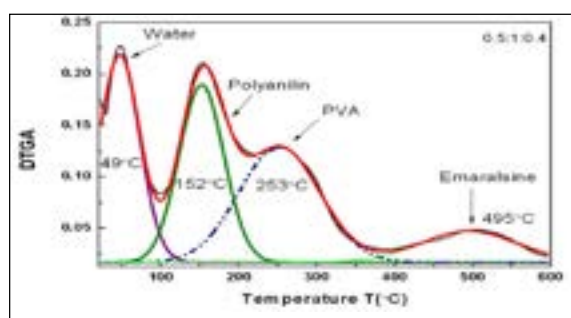


Fig. 2. Peaks separation of the PANi/PVA/CaO nanocomposite

Figures (3A and 3B) showed the TGA and DTGA curves for the three hybrid nanocomposites S1, S2 and S3. All samples have the same thermal decomposition behavior but the sample S2 was more stable than the other samples. Also, S1 showed two

extra peaks at 75 °C and 125 °C indicating that the high concentration of PANi causes trapping for some water molecules in the structure of the nanocomposites. From the DTGA curve, we could confirm that the presence of CaO nanoparticles in the polymeric matrix improved the thermal stability of the protonated PANi.

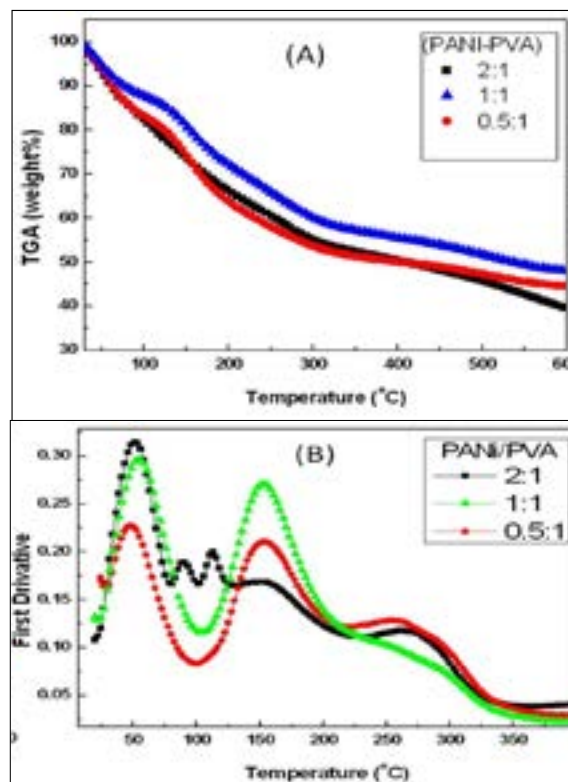


Fig. 3. (A) TGA and (B) DTGA curves for the nanocomposites S1, S2 and S3.

### Electrical Properties

DC and AC measurements were carried out using Keithley 4200-SCS semiconductor characterization unit. The capacitance ( $C$ ) and the impedance ( $Z$ ) of the prepared nanocomposites were measured at frequency changing from  $10^3$  Hz to  $10^6$  Hz at 27 °C. The dielectric constant ( $\epsilon$ ) was estimated by the equation  $\epsilon = C d / \epsilon_0 A$ , where  $C$  is the capacitance (F),  $\epsilon_0$  is the permittivity of the free space ( $8.854 \times 10^{-12}$  F m<sup>-1</sup>),  $A$  is the surface area (m<sup>2</sup>), and the parameter  $d$  is the thickness (m) of the material. The dielectric loss tangent was directly obtained from the instrument. The samples were placed between two copper sheets to make electrical contact with the surface of the samples. The

current-voltage characteristic curves for the samples were carried out in the range of +0.1 to -0.1 V. The absolute values for the electric current were directly calculated by the instrument.

**Voltage–current characteristic curves**

The I-V characteristics were carried out to investigate the electrical conductivity of the three hybrid nanocomposites. Figure (4) shows the I-V curves of the nanocomposites over a DC-voltage range from + 0.1V to -0.1V in cyclic manner. The measurements were repeated several times to ensure that the values were consistent and the average values were represented in Figure (4).

The nanocomposites S1 and S2 showed no hysteresis-curve during the voltage full cycle (voltage increase and decrease) while the nanocomposite S3 showed a hysteresis-curve during the same voltage cycle. This I-V hysteresis could be attributed to the difference in the weight ratio of insulating polymer (PVA) which represents its maximum ratio in the sample S3.

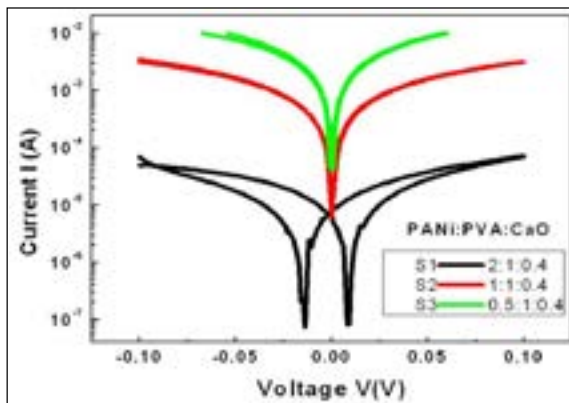


Fig. 4. I-V curves of the nanocomposites S1, S2 and S3.

The existence of PVA with large weight ratios increased the probability of the existence of insulating islands which represents the optimum conditions for charge accumulation during the increase of the applied voltage in certain direction and permits the flow of such accumulated charge during applying the opposite voltage (other direction) causing the appearance of the hysteresis. In addition, such PVA islands could be considered as a source of trapping defect for the charge

carrier, which represents a source of electrical hysteresis. Another contribution for the large weight ratio of PVA in the sample S3 was the encapsulation effect for CaO nanoparticles, which increased the number of charge accumulation centers and reduced the three-dimension network to take place. However, the electrical conductivity of the nanocomposite S3 was in the semiconductor range while the nanocomposite S1 showed a semi-metal behavior. Such results represented very interesting outcome, which opens up new horizons for many applications for such three phase composite, especially in the field of electronics and sensors.

From the Log (V) – Log (I) in relation to the three nanocomposites (Figure 5) and by using a suitable predicting fitting we noted that the nanocomposites S1 and S2, which have higher weight ratio of PANi to PVA, obeyed the linear fitting with slope =1.

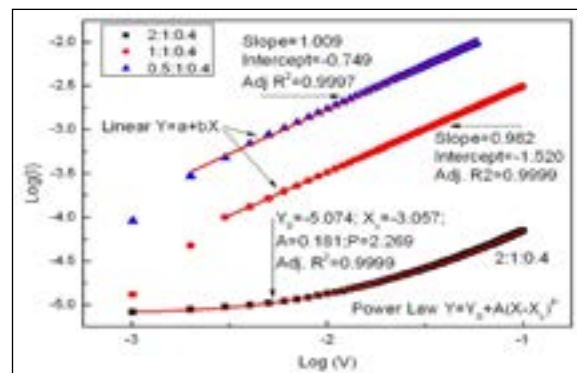


Fig. 5. Log (V)-Log (I) relation for the nanocomposites S1, S2 and S3.

It means that the conduction mechanism of these samples is Ohmic conduction and obeys the equation:  $I = a V^n$ , and  $n=1$  for Ohmic conduction. Also, the nanocomposite S3, which has the higher weight ratio of PVA to PANi, obeyed the power law with “n” greater than two. It indicated that the conduction mechanism of this sample is space charge limiting current. This confirmed the above interpretation for the existence of hysteresis.

**AC characterization**

The frequency dependence of complex impedance for the nanocomposite S1 at various temperatures (from 30 °C to 140

°C) were represented in Figures (6A and 6B) and (7A & 7B); respectively. The values of both real and imaginary parts were strongly affected by temperature. The resistive part ( $Z'$ ) increased with temperature from 30 °C to 80 °C and then decreased monotonically from 90 °C to 140 °C. The spectrum of the imaginary part ( $Z''$  spectrum) followed the same behavior as real part ( $Z'$ ) with a relaxation peak.

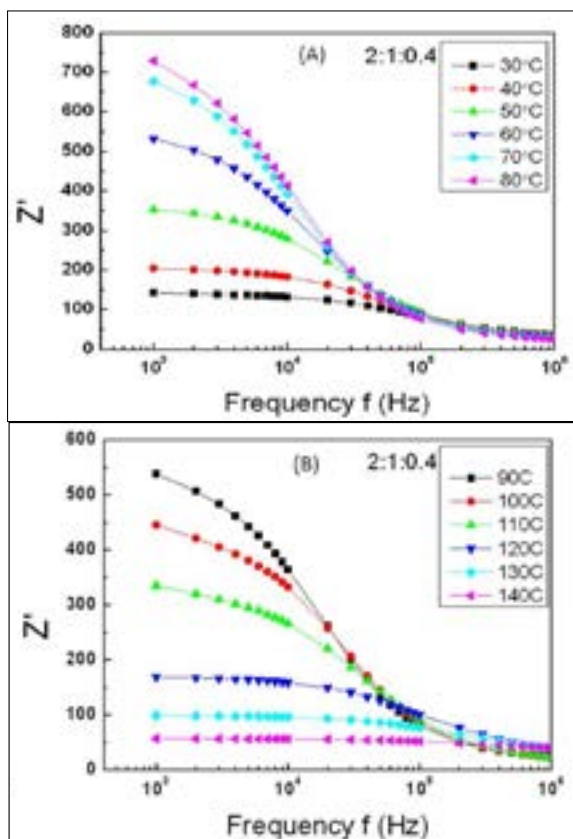


Fig. 6. Relation between the frequency and the impedance  $Z'$  value for S1 at different temperatures.

The relaxation peaks of  $Z''$  were shifted to lower frequency during the first temperature range (30 °C to 80 °C) and to higher frequency during the second temperature range (90 °C to 140 °C). These data showed an interesting feature for these samples and could be explained by considering the water molecules, which adsorbed with the protonated PANi.

It increased the contribution of the ionic conduction at room temperature (Doan *et al.*, 2014). As the temperature increased (30 °C to 90 °C), water molecules evaporated

leading to a reduction in ionic conductivity and an increase in real and imaginary parts. The increase of  $Z'$  was attributed to both a decrease in ionic conduction and formation of electrode polarization (Osman *et al.*, 2012; Ho *et al.*, 2017). For the second temperature range (90 °C to 140 °C),  $Z'$  decreased and the relaxation peaks shifted to a higher frequency. The space charge represented the main contribution for the conduction in this region of temperature beside the contributions of segmental motion, which related to the movement of polymeric chains. Both mechanisms increased the conductivity leading to reduction in both  $Z'$  and  $Z''$ .

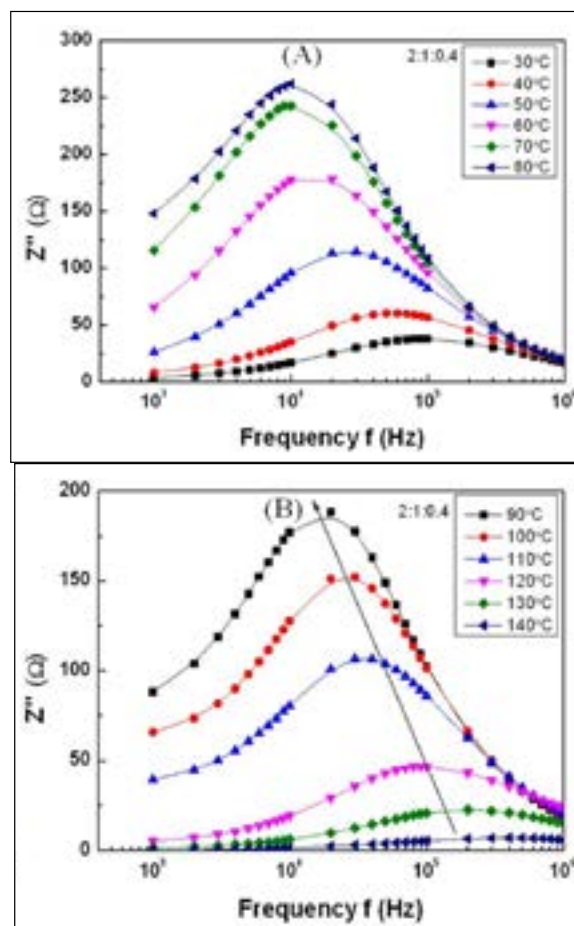


Fig. 7. Relation between the frequency and the impedance  $Z''$  value for S1 at different temperatures.

Figures (8A and 8B) show the AC impedance of the nanocomposite S2 as a function of frequency at different temperatures. The nanocomposite S2 which has equal weight ratio of both PVA and PANi showed that its behavior is different from the previous

nanocomposite S1. Real and imaginary parts increased in the temperature range from 90 °C to 120 °C, while there is no detectable change from 30 °C up to 90 °C. Two overlapped peaks were shown for  $Z''$  at temperatures 100 °C, 110 °C and 120 °C, while single relaxation peaks are shown at 140 °C and 150 °C.

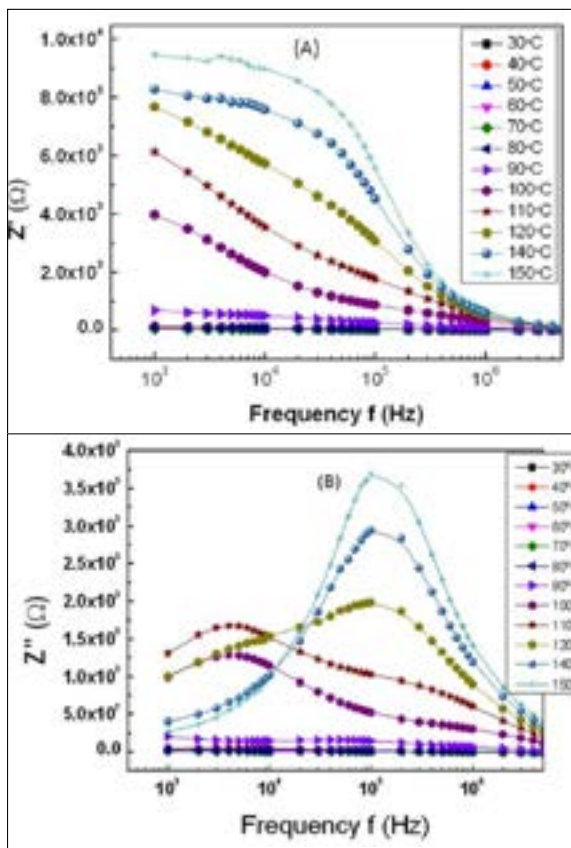


Fig. 8. Relation of the frequency with (a) the impedance value  $Z'$  and (b) the impedance value  $Z''$  for S2 at different temperatures.

Figures (9A and 9B) represent the impedance behavior for the nanocomposite S3. This nanocomposite, which has PVA twice the weight ratio of PANi, exhibited a similar behavior to the second nanocomposite S2. Figure (9A) shows that the real part does not strongly depend on a temperature up to 70 °C. The capacitive component within the sample initiated to improve at the expense of resistance at higher temperatures ( $T > 70^\circ\text{C}$ ). There is no clear and definite electrical relaxation peak for  $Z''(T)$  (Figure 9B). For both the nanocomposites S2 and S3, which have equal or more weight of PVA than PANi,

the blend have some kind of segregation of PVA and PANi. At room temperature, sample contains moisture, which contributed to increase the ionic conduction beside the conduction regions of PANi and PANi-coated CaO. Besides, the sample viscosity was high and the segregation process was neglected (segregation took place at low viscosity state (Narkis *et al.*, 2000)). These factors combined together to increase the sample conductivity for low temperature range. The sample tended to behave as linear resistor with frequency independent behavior. Raising temperature increased the average free volume of the composite constituents and decreased the sample viscosity leading to formation of segregation between its different phases. Both processes acted as a kind of barrier which in turn caused reduction of electrical conductivity ( $Z'$  increased). This could interpret the behavior of  $Z'(f)$  for both nanocomposites S2 and S3.

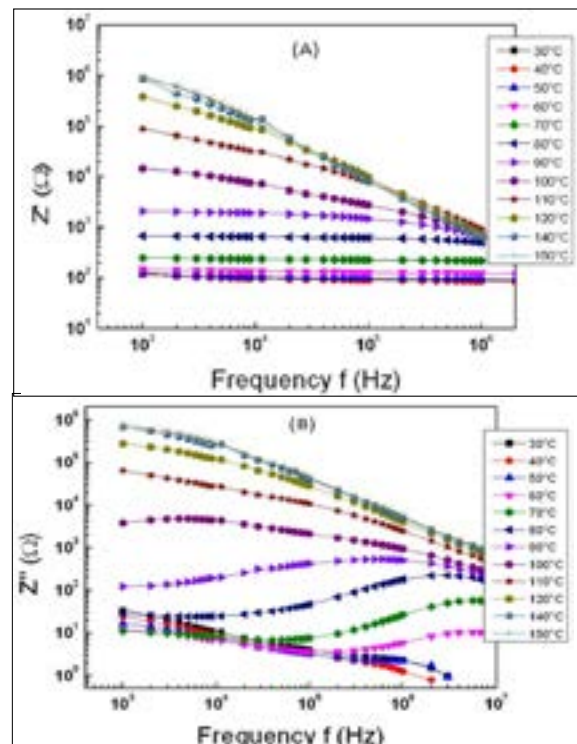


Fig. 9. Relation of the frequency with (a) the impedance value  $Z'$  and (b) the impedance value  $Z''$  for S3 at different temperatures

The imaginary part of  $Z^*$  ( $Z''$ ) increased with temperature for both nanocomposites

S2 and S3. This part ( $Z''$ ) represented the combination of capacitive and resistive components in the samples. The segregation of PVA (insulator) and PANi (conductive) would form a set of capacitors in parallel which accumulated space charge between them. For the nanocomposite S2 and at 100 °C, 110 °C and 120 °C, two relaxation flat peaks were observed which confirmed that there are more than one conduction mechanism while at 140 °C and 150 °C only one clear relaxation appeared. For the nanocomposite S2, a flat relaxation peak at high frequencies shifted to low frequencies with temperature (60 °C to 90 °C) and the sample tended to the pure capacitor behavior at a higher temperature range (110 °C to 150 °C).

## CONCLUSION

The present study achieved a dual effect on the protonated PANi to increase its thermal stability and electrical conductivity through producing three hybrid nanocomposites. In this way, three hybrid nanocomposites (PANi/PVA/CaO) have been prepared and compared with the protonated PANi and its emeraldine base. Thermogravimetric analyses showed that the process of protonation of PANi emeraldine which increased its solubility, reduced its thermal stability. The thermal stability of the protonated PANi was improved and increased by converting the PANi to hybrid nanocomposites indicating that the inclusion of calcium oxide nanoparticles inside the polymers blend (PANi/PVA) enhanced its thermal stability. In addition, the presence of calcium oxide with PVA inside the protonated PANi modified and increased its electrical properties. Furthermore, The I-V characteristic curve showed that the highest concentration of PANi gave a semi-metallic behavior for PVA by applying low voltage values. Moreover, the three hybrid nanocomposites showed different behavior of  $Z'(f)$  and  $Z''(f)$  relations at different temperatures.

## ACKNOWLEDGEMENT

The authors thank the Deanship of Scientific Research in King Faisal University (Saudi Arabia) for funding and providing the facilities required for this research as a part of Annual Research Grants Program (No. 160053).

## REFERENCES

- Afify, T., Ghazy, O., Saleh, H., and Ali, Z. 2018. Efficient in situ synthetic routes of polyaniline/poly (vinyl alcohol)/TiO<sub>2</sub> nanocomposites using gamma irradiation. *J. Mole. Stru.* 1153: 128-134.
- Albu, A.M., Maior, I., Nicolae, C.A., and Bocăneală, F.L. 2016. Novel PVA proton conducting membranes doped with polyaniline generated by *in-situ* polymerization. *Electrochim. Acta.* 211: 911-917.
- Avlyanov, J.K. 1999. Stable polyaniline and polypyrrole nanolayers on carbon surface. *Synthetic metals.* 102: 1272-1273.
- Bhadra, J., Al-Thani, N., Madi, N., and Al-Maadeed, M. 2017. Effects of aniline concentrations on the electrical and mechanical properties of polyaniline polyvinyl alcohol blends. *Arabian J. Chem.* 10: 664-672.
- Breeze, P.A. 1998. Power Generation Technologies: Evaluating the Cost of Electricity. Financial Times Energy. London.
- Daiko, Y., Klein, L.C., Kasuga, T., and Nogami, M. 2006. Hygroscopic-oxides/Nafion hybrid electrolyte for direct methanol fuel cells. *J. Membrane Sci.* 281: 619-625.
- Doan, T.C.D., Ramaneti, R., Baggerman, J., Tong, H.D., Marcelis, A.T.M., and van Rijn, C.J.M. 2014. Intrinsic and ionic conduction in humidity-sensitive sulfonated polyaniline. *Electrochim. Acta.* 127: 106-114.
- Dupare, D., Shirsat, M., and Aswar, A. 2013. Sensing properties of MnO<sub>2</sub>-doped polyaniline / poly vinyl alcohol blend. *Inter. J. Res. in Eng. and Technol.* 2: 308-312.
- Gao, Z., Yang, L., Qin, X., Liu, K., and Gao, Y. 2017. Preparation of semi-insulating PANi/PMMA coating and its applications in internal charging protection. *The Inter. J. Adv. Manuf. Technol.* 96(5-8): 1545-1552

- Ghobadi, S., Mehraeen, S., Bakhtiari, R., Shamloo, B., Sadhu, V., Papila, M., Cebeci, F.Ç., and Gürsel, S.A. 2016. PVA/PANI/rGO ternary electrospun mats as metal-free anti-bacterial substrates. *RSC Advances*. 6: 92434-92442.
- Gök, A., Omastová, M., and Prokeš, J. 2007. Synthesis and characterization of red mud/polyaniline composites: Electrical properties and thermal stability. *European Polymer J*. 43: 2471-2480.
- Graboski, A.M., Ballen, S.C., Manzoli, A., Shimizu, F.M., Zakrzewski, C.A., Steffens, J., and Steffens, C. 2018. Array of Different Polyaniline-Based Sensors for Detection of Volatile Compounds in Gummy Candy. *Food Analytical Methods*. 11: 77-87.
- Guo, Y.N., Gao, Z.Y., Wang, X.X., Sun, L., Yan, X., Yan, S.Y., Long, Y.Z., and Han, W.P. 2018. A highly stretchable humidity sensor based on spandex covered yarns and nanostructured polyaniline. *RSC Advances*. 8: 1078-1082.
- Hatamzadeh, M., Mahyar, A., and Jaymand, M. 2012. Chemical modification of polyaniline by N-grafting of polystyrenic chains synthesized *via* nitroxide-mediated polymerization. *J. Brazilian Chem. Soc*. 23: 1008-1017.
- Hien, H.T., Giang, H.T., Van Hieu, N., Trung, T., and Van Tuan, C. 2017. Elaboration of Pd-nanoparticle decorated polyaniline films for room temperature NH<sub>3</sub> gas sensors. *Sensors and Actuators B: Chemical*. 249: 348-356.
- Ho, K.C., Su, V.C., Huang, D.Y., Lee, M.L., Chou, N.K., and Kuan, C.H. 2017. Investigation of low frequency electrolytic solution behavior with an accurate electrical impedance method. *Chem. Phys. Lett*. 667: 120-123.
- Hoghoghifard, S., Mokhtari, H., and Dehghani, S. 2018. Improving EMI shielding effectiveness and dielectric properties of polyaniline-coated polyester fabric by effective doping and redoping procedures. *J. Ind. Text*. 47: 587-601.
- Jaymand, M. 2013. Recent progress in chemical modification of polyaniline. *Prog. Polym. Sci*. 38: 1287-1306.
- Layeghi, R., Farbodi, M., and Ghalebsaz-Jeddi, N. 2016. Preparation of polyaniline-polystyrene-ZnO nanocomposite and characterization of its anti-corrosive performance. *Inter. J. Nanosci. and Nanotechnol*. 12: 167-174.
- Lesueur, D., Colin, X., Camino, G., and Albérola, N. 1997. Dynamic mechanical behaviour and thermal degradation of undoped polyaniline. *Polym. Bulletin*. 39: 755-760.
- Mat, N.C., and Liong, A. 2009. Chitosan-poly(vinyl alcohol) and calcium oxide composite membrane for direct methanol fuel cell applications. *Eng. Lett*. 116: 1017-1029.
- Narkis, M., Haba, Y., Segal, E., Zilberman, M., Titelman, G., and Siegmann, A. 2000. Structured electrically conductive polyaniline/polymer blends. *Polym. for Adv. Technol*. 11: 665-673.
- Olad, A., and Gharekhani, H. 2016. Study on the capacitive performance of polyaniline/activated carbon nanocomposite for supercapacitor application. *J. Polym. Res*. 23: 1-11.
- Osman, Z., Mohd Ghazali, M.I., Othman, L., and Md Isa, K.B. 2012. AC ionic conductivity and DC polarization method of lithium ion transport in PMMA-LiBF<sub>4</sub> gel polymer electrolytes. *Results in Physics*. 2: 1-4.
- Pingan, H., Mengjun, J., Yanyan, Z., and Ling, H. 2017. A silica/PVA adhesive hybrid material with high transparency, thermostability and mechanical strength. *RSC Advances*. 7: 2450-2459.
- Saadattalab, V., Shakeri, A., and Gholami, H. 2016. Effect of CNTs and nano ZnO on physical and mechanical properties of polyaniline composites applicable in energy devices. *Progress in Natural Science: Materials International* 26: 517-522.
- Salem, M.A., Elsharkawy, R.G., and Hablas, M.F. 2016. Adsorption of brilliant green dye by polyaniline/silver nanocomposite: Kinetic, equilibrium, and thermodynamic studies. *European Polymer Journal* 75: 577-590.
- Shahin, N., El Mongy, S.A., Kamal, R., El-Bially, A., Shabaka, A., and Barakat, F. 2017. Preparation and characterization of polyaniline/polyvinyl alcohol nanocomposite by laser irradiation. *Inter. J. of Basic and Applied Sci*. 6: 77-84.

- Singh, V.P., Ramani, R., Singh, A.S., Mishra, P., Pal, V., and Saraiya, A. 2016. Dielectric and conducting behavior of pyrene functionalized PANI/P (VDF - co - HFP) blend. *J. of Appl. Polym. Sci.* 133. doi.org/10.1002/app.44077.
- Subramanian, E., Ramalakshmi, R.D., Vijayakumar, N., and Sivakumar, G. 2012. Hybrid composite materials of anatase titania and conducting polyaniline: properties and chemical sensor application. *Indian J. of Eng. & Mater. Sci.* 19: 237-244.
- Sultana, S., Khan, M. Z., Umar, K., and Muneer, M. 2013. Electrical, thermal, photocatalytic and antibacterial studies of metallic oxide nanocomposite doped polyaniline. *J. of Mater. Sci. & Technol.* 29: 795-800.
- Sun, J., Shen, Y., and Hu, X.S. 2018. Polyaniline/flower-like CuS composites with improved electromagnetic interference shielding effectiveness. *Polym. Bull.* 75: 653-667.
- Tavares, A.C., Hümmelgen, I.A., and Meruvia, M.S. 2018. All-organic bipolar vertical transistor with sulfonated polyaniline base energy barriers favoring recombination emitter-collector current. *Organic Electronics.* 54: 114-118.

## تحسين الثبات الحراري والخواص الكهربائية للبوليمر أنيلين من خلال التركيبات النانوية المهجنة

أسامة صابر و صبحي إبراهيم و محمد أبو عابدين و عادل الشعبي و عبد الله النعيم

قسم الفيزياء، كلية العلوم، جامعة الملك فيصل  
الأحساء، المملكة العربية السعودية

استلام 9 مايو 2018م - قبول 2 يناير 2019م

### الملخص

البوليمر المنفرد لا يستطيع تحقيق متطلبات التقدم التقني الحالي؛ لذلك فإن اتحاد أكثر من بوليمر عضوي مع أكاسيد الفلزات غير العضوية يؤدي إلى بوليمرات ذات خصائص مميزة ومفضلة عنها وهي منفردة، وبالتالي هذه الدراسة تهدف إلى تحسين كل من الخواص الكهربائية والثبات الحراري للبوليمر أنيلين من خلال تحضير ثلاثة تركيبات مهجنة من المركبات العضوية وغير العضوية؛ ولذلك تم تحضير ثلاثة تركيبات نانوية بنسب وزنية مختلفة بين البوليمر أنيلين والبوليمر الفينيل الكحولي مع نسبة ثابتة من حبيبات أكسيد الكالسيوم النانوية.

أثبتت التحاليل الحرارية أن هذه التركيبات لها ثبات حراري أعلى من البوليمر أنيلين المدعم بالبروتونات، ومن التوصيف الكهربائي للتيار المتردد والتيار الثابت عند درجات الحرارة المختلفة، وأظهرت أن العينات ذات النسبة العالية من البوليمر أنيلين جعلت قدرة التوصيل الكهربائي للبوليمر الفينيل الكحولي العازل قريب من التوصيل الكهربائي للمعادن، وكذلك أظهرت نتائج مشيرة للاهتمام عند دراسة العلاقة بين عوامل التيار الكهربائي المتردد ("Z & Z") مع تردد التيار الكهربائي. هذه النتائج تفتح آفاقاً جديدة في مجال الإلكترونيات والحساسات والمجسات.

الكلمات المفتاحية: أكسيد الكالسيوم، بولي أنيلين، بولي فينيل الكحولي، تركيبات نانوية، الثبات الحراري، الخواص الكهربائية.